Scientific Reports

https://doi.org/10.1038/s41598-026-45185-x

Article in Press

Multi-objective techno-economic and environmental optimization of hydrogen-based hybrid renewable energy system using osprey optimization algorithm

Received: 18 January 2026

Accepted: 17 March 2026

Published online: 02 April 2026

Cite this article as: Ermiş S., Taşdemir O. & Al-Hajj R. Multi-objective techno-economic and environmental optimization of hydrogen-based hybrid renewable energy system using osprey optimization algorithm. *Sci Rep* (2026). https://doi.org/10.1038/s41598-026-45185-x

Salih Ermiş, Oğuz Taşdemir & Rami Al-Hajj

Article

Multi-Objective Techno-Economic and Environmental Optimization of Hydrogen-Based Hybrid Renewable Energy System Using Osprey Optimization Algorithm

Salih ERMİŞ [1], Oğuz TAŞDEMİR [1], Rami AL-HAJJ[2,*]

[1] Department of Electrical and Electronics Engineering, Faculty of Engineering and Architecture, [1]Kırşehir Ahi Evran University, Kırşehir, Türkiye;
[2] College of Engineering and Technology, American University of the Middle East, Kuwait;

* Correspondence: rami.alhajj@aum.edu.kw

Abstract: The intermittent nature of renewable energy sources poses significant challenges for continuous power supply, necessitating the integration of robust energy storage and optimization systems. While hybrid renewable energy systems (HRES) offer a sustainable solution, achieving an optimal sizing that simultaneously minimizes economic costs and health-damaging carbon emissions remains a complex nonlinear challenge. This study proposes a comprehensive multi-objective optimization framework for a grid-connected HRES integrating photovoltaic (PV), wind turbine (WT), fuel cell (FC), electrolyzer, and hydrogen storage components. The Osprey Optimization Algorithm (OOA) is applied to optimize system sizing and power management. The primary objectives are to concurrently minimize the Cost of Energy (COE) and the Human Health Damage (HHD) due to lifecycle emissions, while ensuring strict system reliability (Loss of Power Supply Probability, LPSP = 0) using one-year meteorological data from Central Anatolia, Türkiye. Comparative analyses demonstrate that OOA exhibits superior performance in terms of solution quality and computational efficiency compared to PSO, TLBO, and GWO algorithms. Among the simulated scenarios (PV/WT/FC, PV/FC, and WT/FC), the PV/WT/FC configuration provides the most balanced Pareto-optimal solution. It achieves the lowest environmental impact with an HHD of 0.419 DALY and a highly competitive COE of 0.238 $/kWh. The integration of hydrogen production and storage effectively mitigates renewable intermittency, reducing grid dependency and emissions. The OOA is confirmed as a highly robust optimization tool, providing decision-makers with a cost-effective and environmentally sustainable framework for designing modern hybrid power systems.

Keywords: Hybrid Renewable Energy System, Osprey Optimization Algorithm, Hydrogen Energy, Techno-Economic Analysis, Environmental Sustainability

1. Introduction

The rapid increase in energy demand, technological advancements, depletion of fossil fuel reserves, and concerns regarding environmental sustainability have made the integration of renewable energy sources into power systems inevitable [1, 2]. The use of fossil fuels for electricity generation has led to serious greenhouse gas emissions and environmental degradation, posing a significant threat to the future [3]. The European Union aims to increase the share of renewable energy in total generation to 42.5% by 2030, while the United States has set a target of 80% by the same year [1]. Likewise, in Türkiye, the use of renewable energy resources has been gaining increasing importance due to their sustainability, environmental friendliness, and contribution to reducing ecological problems [4]. In this context, solar photovoltaic (PV) and wind turbine (WT) systems are among the most widely utilized renewable energy technologies due to their environmentally friendly and inexhaustible characteristics [5]. However, because these resources are inherently intermittent and variable, they create significant uncertainty regarding continuous energy supply. Therefore, hydrogen-based energy storage technologies (particularly those involving electrolyzers, fuel cells (FC), and hydrogen tanks) play a key role in enhancing the stability of hybrid renewable energy systems (HRES) [6, 7]. Hybrid power systems, which combine multiple energy sources with different production profiles, can enhance both energy continuity

and overall system efficiency. Since these systems rely on renewable resources, they not only increase electricity production but also reduce carbon emissions and environmental pollution [8]. Numerous generation configurations can be utilized in hybrid system design, with each configuration optimized to ensure maximum efficiency and continuous operation. PV systems maximize energy production during high solar irradiation periods, while WT systems generate power when wind potential is strong. The fuel cell and electrolyzer units store excess renewable energy in hydrogen form and reconvert it into electricity when production decreases. Consequently, the system attains a flexible and stable structure for meeting the load demand [9, 10]. The design of hybrid renewable energy systems is a complex multi-parameter optimization problem involving various technical and operational constraints. The primary objectives in these systems are to minimize both, the cost of energy (COE) and the human health damage (HHD) caused by emissions while maintaining self-sufficiency and reducing grid dependency. Therefore, researchers have increasingly adopted multi-objective optimization approaches to balance the economic and environmental performance metrics. For this purpose, several metaheuristic algorithms such as Genetic Algorithm (GA) [11], Particle Swarm Optimization (PSO) [12], and Artificial Bee Colony (ABC) [13] have been employed for the optimal sizing, techno-economic analysis, and performance evaluation of HRESs. For example, we describe the use of an effective metaheuristic method based on Artificial Bee Swarm Optimization (ABSO) for the design of a hybrid renewable energy system incorporating photovoltaic, wind, hydrogen, and reverse osmosis desalination technologies. This system aims to both increase freshwater resources and meet the energy needs of an independent region in Iran. [14]. In another study, multiple algorithms such as the Water Cycle Algorithm (WCA), Moth-Flame Optimization (MFO), Whale Optimization Algorithm (WOA), and Hybrid PSO–Gravitational Search Algorithm (PSOGSA) were applied to determine the optimal component sizes of an off-grid PV/WT/diesel/battery system that minimizes energy cost and loss of power supply probability [15]. Similarly, a sizing model was developed for a hybrid renewable energy system (HRES) consisting of PV, wind turbine (WT), diesel generator (DG), and battery components. This model uses a hybrid AI algorithm consisting of Enhanced Differential Evolution (ED) and Particle Swarm Optimization (PSO) techniques to determine the optimal sizing for each component. It also provides designers with a variety of options to choose from based on their preferences, considering different optimization objectives [16]. Two different optimization algorithms, such as Genetic Algorithm (GA) and Particle Swarm Optimization (PSO), were applied to obtain the optimum design of the hybrid PV/WT/Biomass production system to reduce the energy costs [17].

For hybrid PV-hydrogen systems, PSO has been used to minimize both energy costs and CO_2 emissions [18]. The Differential Evolution Algorithm (DEA) was employed to design an off-grid PV/WT/FC system that minimizes total system costs over its lifetime [19]. In India, a hybrid WCA–MFO method was used to design an off-grid PV/biogas/pumped-hydro/battery hybrid system for a radio transmitter station, demonstrating significant techno-economic advantages [20]. Additionally, the optimal configuration of a standalone hybrid PV/WT/FC energy system for a small-scale area in Egypt was achieved using the Firefly Algorithm (FA). In this study, the main objective function is to minimize the total annual cost of the hybrid system. The optimization results obtained with FA were compared with the those obtained by the Shuffled Frog Jumping Algorithm (SFLA) and PSO [21]. In a study considering socio-demographic factors, a combination of Genetic Algorithm (GA) and exhaustive search technique was applied for the optimal sizing of a standalone hybrid PV/WT/battery system. The primary objective of this optimization study is to ensure system reliability by meeting the load demand while minimizing the total cost (TC) [22]. To ensure effective microgrid management using various renewable energy sources, a system model was developed considering uncertainties in production. Minimizing the cost of energy (COE) was achieved using a novel optimization method based on the Bat Algorithm [23]. In Algeria, PSO was applied to optimize a PV/diesel/battery hybrid system while considering the loss of power probability [24]. In Morocco, a Modified PSO (MPSO) algorithm combined with Six Sigma tools was used for rural electrification planning, achieving minimized Net Present Cost (NPC), COE, and greenhouse gas emissions [25]. The

Firefly Algorithm (FA) was applied to solve the design problem of a hybrid energy system. This study determined the optimal system combination that meets reliability constraints while minimizing costs. The results demonstrated a feasible design for a maximum load loss limit of 3%, and the PV/WT/battery combination was identified as the lowest-cost option [26]. Despite the extensive literature on HRES optimization, critical research gaps remain. First, while economic indicators and basic CO_2 emissions are widely utilized, comprehensive environmental metrics such as Human Health Damage (HHD) expressed in DALYs are rarely integrated into the multi-objective sizing of hydrogen-based systems. Second, classical heuristic algorithms (e.g., PSO, GA) frequently suffer from premature convergence and easily get trapped in local optima when dealing with the highly nonlinear, multi-dimensional search spaces typical of grid-connected PV/WT/FC configurations. To address these gaps, this study introduces a novel approach by simultaneously evaluating economic (COE) and direct human health impacts (HHD). In this study, a multi-objective optimization approach based on the Osprey Optimization Algorithm (OOA) is applied to a PV/WT/FC hybrid system to minimize COE and HHD simultaneously. The system simulation is conducted for a location in Central Anatolia, Türkiye, using one-year meteorological and load data. Three different configurations - PV/WT/FC, PV/FC, and WT/FC - were analyzed, and the results were compared against those obtained from PSO, TLBO, and GWO algorithms. This study provides a new perspective on the optimal design of hybrid PV/WT/FC systems by combining economic and environmental objectives within a unified optimization framework using OOA. The results contribute significantly to sustainable energy planning and the development of low-carbon hybrid power systems.

The main contributions and original aspects of this research can be summarized as follows:

- The hybrid system integrating PV, WT, FC, electrolyzer, and H_2-tank components was dynamically modelled in MATLAB, and an annual (8,760-hour) simulation was conducted.
- The system performance was analyzed under economic (COE) and environmental (HHD) objectives using a multi-objective optimization framework.
- Highlighting the methodological novelty of this work, the recently developed Osprey Optimization Algorithm (OOA) is applied for the first time to optimize a complex grid-connected PV/WT/FC system, effectively overcoming the local optima limitations of classical algorithms (PSO, TLBO, and GWO).
- The developed power management strategy ensured LPSP = 0, directing excess renewable energy to hydrogen storage, thus enhancing system reliability.
- The grid-connected model improved load coverage and reliability, though greater higher grid dependency increased carbon emissions. The PV/WT/FC configuration yielded the lowest LCE and HHD values, indicating minimal reliance on the grid.

The results demonstrate that a multi-objective optimization approach that simultaneously minimizes economic and environmental indicators can serve as a reference model for sustainable hybrid energy planning.

2. Calculation Method

2.1. Hybrid System Model and Operating Strategy

In this study, a hybrid renewable energy system (HRES) consisting of photovoltaic (PV) panels, wind turbines (WTs), fuel cells (FCs), and an electrolyzer for hydrogen production is designed. The schematic diagram of the HRES is presented in Figure 1. The system operates in on-grid mode and is analyzed under different operational scenarios.

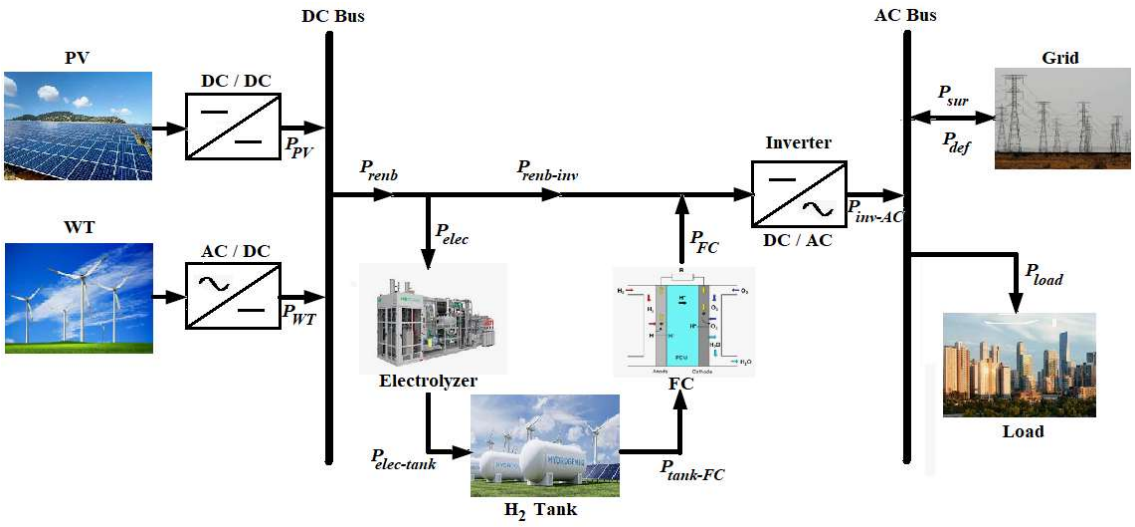

Figure 1. Schematic diagram of the grid-connected PV/WT/FC HRES

The operational strategy of the proposed HRES is defined in three main stages:

When renewable energy generation equals the load demand, the system supplies the load entirely using PV and WT generation without requiring support from the FC or the grid. In this case, the inverter efficiency (η_{inv}) ensures that renewable power is directly delivered to the load. $P_{renb}(t) = P_{load}(t)/\eta_{inv}$

When renewable energy generation exceeds the load demand, $P_{renb}(t) > P_{load}(t)/\eta_{inv}$, the surplus renewable energy is transferred to the electrolyzer, where it is converted into hydrogen and stored in the H_2 tank. After supplying the load, any remaining energy is sold to the grid (Grid Sale).

$P_{sale}(t) = P_{renb-inv}(t) \times \eta_{inv} - P_{load}(t)$

When renewable energy generation is lower than the load demand, $P_{renb}(t) < P_{load}(t)/\eta_{inv}$ the power deficit is compensated first by the fuel cell. If the FC output is insufficient to meet the demand, the remaining power is purchased from the grid (Grid Buy).

$P_{buy}(t) = P_{load}(t) - P_{inv-AC}(t)$

The flowchart of the proposed operating strategy is illustrated in Figure 2. The diagram explicitly details the hierarchical decision-making process for real-time power balancing. Specifically, it visually delineates the 'Deficit' branch where, if the Fuel Cell (FC) output is insufficient to meet the load demand due to hydrogen limitations or capacity constraints, the system automatically triggers the 'Grid Buy' mechanism. This ensures that the grid acts as the ultimate backup to cover any remaining power deficit, thereby guaranteeing that the load is fully met (LPSP = 0) at every time step, strictly aligning with the system reliability constraints described in this section.

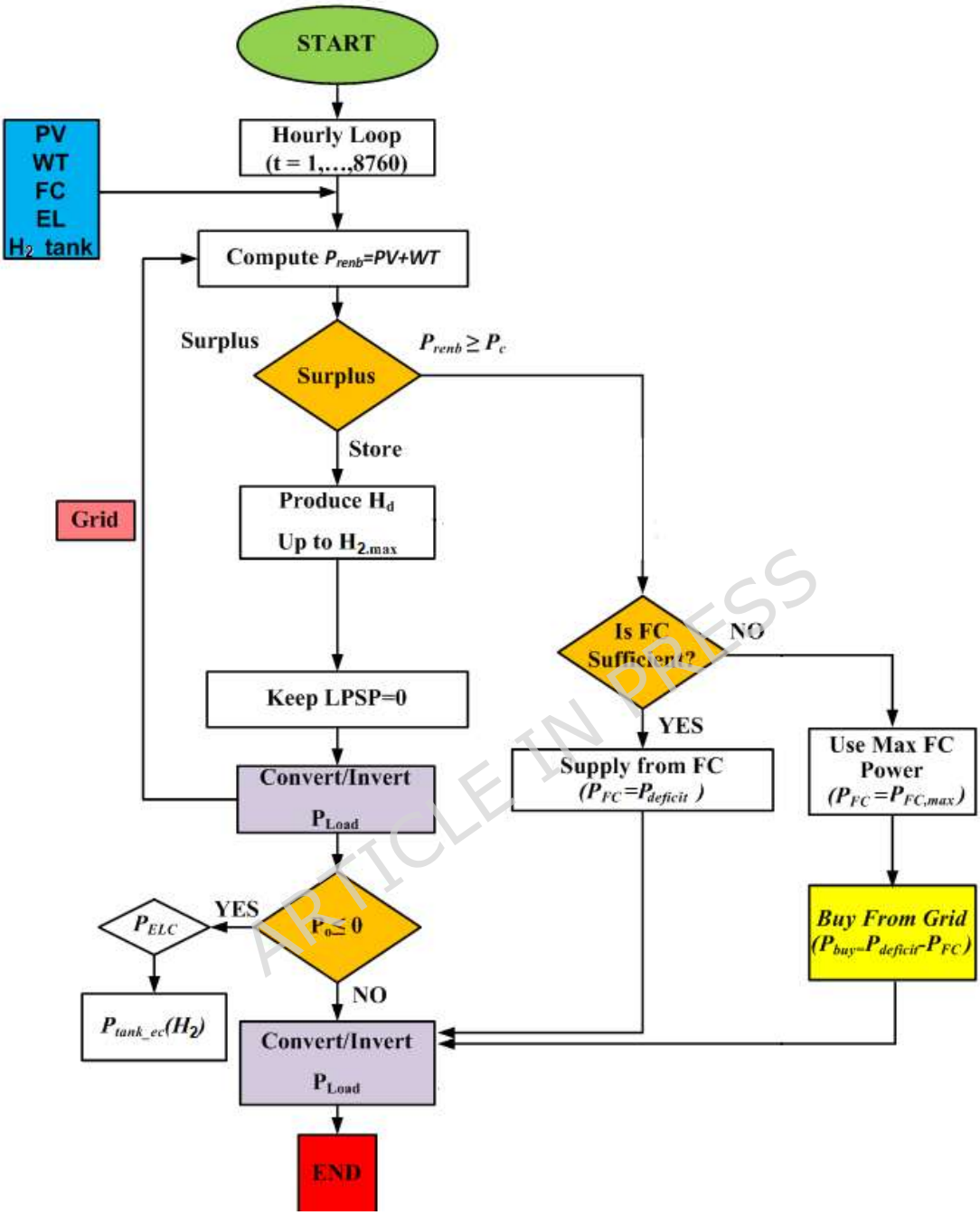

Figure 2. Flowchart of the proposed operational strategy.

In this strategy, energy balance is achieved dynamically. During high renewable production periods, hydrogen storage plays a crucial role in absorbing excess energy, while during low renewable availability, the FC efficiently converts stored hydrogen into electricity. This mechanism ensures a continuous supply and minimizes grid dependency. Overall, the proposed PV/WT/FC–H_2 hybrid system provides operational flexibility, reliability, and sustainability by integrating renewable generation with hydrogen-based energy storage and conversion units.

3. Formulation of the Problem

3.1. System Models

3.1.1. PV Model

Photovoltaic (PV) systems consist of semiconductor devices that directly convert solar radiation into electrical energy through the photovoltaic effect. Typically, PV modules are composed of silicon-based solar cells. Their output depends on both environmental and physical parameters, which can be modelled mathematically to predict energy production [27]. The operating cell temperature (Tc) of the PV module is calculated using the Nominal Operating Cell Temperature (NOCT) method. In this approach, NOCT is a manufacturer-specified parameter (typically 45 °C), while the instantaneous cell temperature is derived based on the ambient temperature (Ta) and solar irradiance (I_T), as shown in Equation 1 [28, 29].

$$Tc = Ta + \frac{(NOCT-20)}{800} \cdot I_T \quad (1)$$

Here, $NOCT$ represents the nominal operating temperature of the panel (45 °C), Ta represents the ambient temperature (°C), and I_T represents the instantaneous solar radiation (W/m²). The cell temperature change is corrected for the panel efficiency using the temperature coefficient (α_p). The temperature correction factor is shown in Equation 2 [30].

$$f_{temp} = 1 + \alpha_p.(T_c - 25) \quad (2)$$

where α_p indicates that the panel efficiency decreases with increasing temperature. The instantaneous output power of the PV system, $P_{PV}(t)$, is calculated as shown in Equation 3 [29].

$$P_{PV}(t) = N_{PV}.P_{unit}.\eta_{PV}.f_{PV}.\frac{I_T}{1000}.\max(0, f_{temp}) \quad (3)$$

where N_{PV} is the number of PV panels, P_{unit} is the nominal power of a panel, η_{PV} is the efficiency of the panel, f_{PV} is the performance ratio of the panel.

This model takes into account the effects of temperature and radiation on PV generation, and the $\max(0, f_{temp})$ function is applied to prevent negative values. Thus, the hourly power generation profile of the PV system is obtained based on solar radiation and temperature conditions.

3.1.2. WT Model

WT systems convert wind energy into mechanical energy, which is then converted into electrical energy by generators. WT models are expressed by mathematical equations that account for the interactions of aerodynamic, mechanical, and electrical components. WT systems rotate by harnessing the wind kinetic energy, and this rotational motion is converted into electrical energy by the generator [31]. The nominal output power of the WT is calculated according to Equation 4.

$$P_{WT}(t) = N_{WT}.P_{WT-gen} \quad (4)$$

Here, N_{WT} represents the number of wind turbines. The efficiency of a WT depends on the design of the rotor blades, the wind speed, and the generator's efficiency. The power of a WT is proportional to the third power of the wind speed. The factors that determine the output power of a wind turbine are:

- Cut-in speed (V_{cut-in}): Minimum speed at which the turbine starts generating power.
- Rated speed (V_{rated}): Speed corresponding to the maximum rated output.
- Cut-out speed ($V_{cut-out}$): Maximum allowable wind speed before shutdown.

Mathematically, the WT output power is expressed in Equation 5 as follows:

$$P_{WT-gen} = \begin{cases} 0 & V < V_{cut-in}, V > V_{cut-o} \\ P_{WT-rated}\left(\frac{V-V_{cut-i}}{V_{rated}-V_{cut-in}}\right)^3 & V_{cut-in} \le V < V_{rated} \\ P_{WT-rated} & V_{rated} \le V < V_{cut-out} \end{cases} \quad (5)$$

Here; P_{WT-ge} is defined as WT output power, $P_{WT-rated}$ is represents the rated (nominal) power of the turbine, V is wind speed, V_{cut-in} is initial wind speed, V_{rated} is nominal wind speed, $V_{cut-out}$ is cut-off wind speed [32, 33].

3.1.3. Electrolyzer Model

Electrolyzers are devices that split water into hydrogen and oxygen gases using electrical energy. In hybrid power systems, electrolyzers are used to store excess renewable energy in the form of hydrogen [34]. The electrolysis process is based on the following chemical reaction Equation 6.

$$H_2O + extElectricalEnergy \rightarrow H_2 + \frac{1}{2}O_2 \quad (6)$$

Electrolyzer power is calculated as in Equation 7, taking into account the excess energy $P_{surplus}$ and electrolyzer capacity $P_{EL,max}$.

$$P_{EL}(t) = \min(P_{EL,max}, P_{surplus}(t)) \quad (7)$$

3.1.4. Hydrogen Tank Model

Hydrogen tanks are systems that provide safe and efficient storage of hydrogen produced by electrolysis. Hydrogen storage in hybrid power systems optimizes energy management by increasing the availability of excess renewable energy. The energy stored in the hydrogen tank is given in Equation 8.

$$H_2(t) = H_2(t-1) + \left(P_{EL}(t) - \frac{P_{ta}\quad(t)}{\eta_{storage}}\right) \times \Delta t \quad (8)$$

Here, P_{tank-} is defined as the power transferred from the hydrogen tank to the fuel cell, $\eta_{storage}$ is the hydrogen storage efficiency, and Δt is the step time [35]. The mass of hydrogen stored in the tank is calculated using Equation 9:

$$M_{tank}(t) = \frac{E_{H_2-tank}(t)}{HHV_{H_2}} \quad (9)$$

Here, the hydrogen high heating value HHV_{H_2} is selected as 39.7 kWh/m2 [36]. The boundaries of the tank must be determined to ensure that the pressure in the hydrogen tank does not fall below a minimum level or exceed the maximum.

$$M_{tank,min} \leq M_{tank} \leq M_{tank,max} \quad (10)$$

3.1.5. FC Model

FCs are electrochemical devices that convert chemical energy directly into electrical energy. They typically generate electricity using hydrogen fuel, generating only byproducts such as water and heat. Therefore, FCs offer an ideal solution for clean energy systems that reduce carbon emissions [37]. Because the output of PV and WT renewable energy units depends on weather conditions, FCs provide an alternative power source as backup units. FCs generate electricity through the chemical reaction of hydrogen and oxygen. The electrical energy generated from this reaction can be used to power loads directly or to direct energy storage systems. The output power of an FC is expressed by Equation 11.

$$P_{FC}(t) = min\left(P_{FC,max}, \frac{H_2(t)}{\eta_{FC} \cdot HHV_{H2}}\right) \quad (11)$$

Here, η_{FC} is the electrical efficiency of FC [38, 39].

3.1.6. Inverter Model

Inverters are power electronic devices that convert direct current (DC) to alternating current (AC). In hybrid energy systems, inverters convert DC electricity generated from PV panels, fuel cells, and battery systems into AC power suitable for the grid or load. The AC power transferred from the inverter to the load is defined by Equation 12:

$$P_{inv} = (P_{FC} + P_{PV} + P_{WT}) \times \eta_{inv} \quad (12)$$

Here, η_{inv} is the inverter efficiency. Inverter efficiency varies depending on the load and operating conditions and can typically be between 90% and 98% [40].

3.2. Objective Function

In this study, the objective function is designed to optimize the operation of a hybrid renewable energy system consisting of PV panels, WT, FC, and an electrolyzer for hydrogen production. The objective is achieved through a multi-objective optimization approach that simultaneously minimizes two key performance indicators. The function defined for this purpose is determined by Equation 13. The techno-economic-environmental data coefficient values for all components of the HRES system in the optimization study are given in Table A. Specifically, regarding the grid interaction limits presented in Table A, a deliberate disparity between the purchase (0.12 $/kWh) and sell-back (0.05 $/kWh) prices is maintained. This assumption reflects real-world market dynamics where the purchase price corresponds to the retail electricity rate (including taxes and distribution fees), while the sell-back price represents the lower wholesale market clearing price or feed-in tariff. This approach prevents the overestimation of economic benefits derived from grid sales and ensures a realistic and conservative techno-economic assessment.

$$minF(x) = [COE(x), HHD(x)] \quad (13)$$

Here, COE (Cost of Energy, $/kWh) represents the levelized cost of energy produced, HHD represents Human Health Damage, and x represents the decision variable Equation 14.

$$x = [N_{PV}, N_{WT}, P_{FC}, H_2, P_{EL}] \quad (14)$$

3.2.1. Cost of Energy (COE)

The system's unit energy cost is calculated by taking into account total investment (C_{cap}), operation and maintenance (O&M) costs, renewal costs, network purchase and sale transactions, and economic life. First, Net Present Cost (NPC) is defined using Equation 15 as follows [41].

$$NPC = \sum_{i\epsilon\{PV,WT,FC,H_2,Inv\}}\left(C_{cap(i)} + C_{OM(i)} + C_{rep(i)}\right) + C_{grid} \quad (15)$$

Here, for each model, the investment costs (C_{cap}), operational maintenance costs (C_{OM}), replacement costs (C_{rep}), and the difference between the cost paid for energy purchased from the grid and the revenue obtained for energy sold to the grid (C_{grid}) constitute the total cost. The initial investment cost (C_{cap}) represents the total investment cost required for the initial installation of the system and is calculated as follows Equation 16.

$$C_{cap} = \sum_{i=1}^{N} C_i \times P_i \quad (16)$$

Here, C_i is the unit cost per model ($/kW or $/kg), P_i is the model capacity (kW or kg), and N is the number of models in the system. This equation calculates the total initial investment cost based on the unit costs and capacities of all components in the system. Operation and maintenance cost (C_{OM}) represents the regular maintenance and operation costs incurred during system operation. It is calculated using Equation 17 as follows:

$$C_{OM} = \sum_{i=1}^{N} OM_i \times P_i \quad (17)$$

Here, OM_i represents the annual operating and maintenance cost ($/kW or $/kg) per model. This equation calculates the total annual operating expenses by including the annual operating and maintenance costs of all components. The replacement cost (C_{rep}) represents the cost required to replace system components at the end of their economic life. It is calculated using Equation 18, as shown below.

$$C_{rep} = \sum_{i=1}^{N} \frac{R_i \times P_i}{L} \quad (18)$$

Here, R_i is defined as the replacement cost per component ($/kW or $/kg) and L is the economic life of the component (years). This equation determines how often system components need to be replaced throughout their lifetime and, accordingly, the annual replacement cost. The Capital Recovery Factor (CRF) is shown in Equation 19 [42].

$$CRF = \frac{r(1+r)^L}{(1+r)^L-1} \quad (19)$$

Here, r is the interest rate (chosen as 0.05 in this study), L is the economic life of the system components (years). Unit energy cost (COE) is defined by Equation 20 [43].

$$COE = \frac{NPC.CRF}{E_{served}} \quad (20)$$

Where E_{served} is the annual total amount of energy provided by the system to the consumer.

3.2.2. Human Health Damage (HHD)

The environmental performance of the hybrid energy system was assessed by calculating the total carbon emissions caused by the system components throughout their life cycle. The indicator used for this purpose is Life Cycle Emissions (LCE), which is the sum of emissions from PV, WT, FC, electrolyzer (EL), and grid sources, defined by Equation 21 [44].

$$LCE = E_{PV}.\varepsilon_{PV} + E_{WT}.\varepsilon_{WT} + E_{FC}.\varepsilon_{FC} + E_{EL}.\varepsilon_{EL} + E_{grid}.\varepsilon_{grid} \quad (21)$$

Here, E_i represents the annual energy flows of the i^{th} system component, and ε represents the emission coefficient per unit energy of each component. The emission coefficients (ε) of the system components are shown in Table A.

PV-related emissions arise from the panel production, transportation, and installation stages; WT emissions arise from turbine manufacturing and maintenance processes; and FC emissions arise from indirect effects during the conversion of hydrogen into electricity. The electrolyzer emission value is assumed to be zero because the system achieves carbon-neutral production when fed with a surplus of renewable energy. Conversely, grid-related emissions contribute the most to the system's total carbon load due to the predominance of fossil-based generation.

The HHD metric, representing health impact, was used as the environmental performance indicator. This value was obtained by multiplying the total life-cycle emissions (LCE) from the system by the conversion factor for health impacts, as in Equation 22 [45].

$$HHD = LCE.\alpha \quad (22)$$

The coefficient used here is α =1.4×10^{-6} DALY/(kg CO_2-eq). Thus, the HHD value represents the annual impact of greenhouse gas emissions caused by system components on human health [46].

The environmental impact analysis quantitatively demonstrated the hybrid energy system's component-by-component emission profile and health impacts. These values were optimized using the economic indicator Cost of Energy (COE) to obtain Pareto-optimal solutions. Thus, a multi-objective sustainability analysis based on the cost-emission balance was conducted.

3.3. System Constraints

The optimization of the hybrid PV/WT/FC energy system was carried out under constraints defined by the technical, operational, and energy balance conditions of the system components. These constraints ensure both the physical feasibility of the system and the continuity of the energy supply-demand balance.

3.3.1. Decision Variable Limits

The five decision variables used in the optimization; number of photovoltaic panels (N_{PV}), number of wind turbines (N_{WT}), fuel cell power (P_{FC}), hydrogen storage capacity (H_2) and electrolyzer capacity (P_{EL}) were selected between the following lower and upper limits:

$0 \le N_{PV} \le 2000,\ 0 \le N_{WT} \le 200,\ 0 \le P_{FC} \le 150,\ 0 \le H_2 \le 600,\ 0 \le P_{EL} \le 120$

These limits represent the economic and technical capacity limits of the system components.

The rationale behind these specific bounds is grounded in both mathematical flexibility and practical site constraints. The lower bound for all decision variables is set to zero, which allows the optimization algorithm to freely evaluate various system configurations by potentially omitting certain components (e.g., sizing a WT/FC system without PV arrays). Conversely, the upper bounds are defined based on physical and economic feasibility. Specifically, the maximum capacities for the PV and WT units are constrained by the available land area at the deployment site. Meanwhile, the upper limits for the fuel cell, electrolyzer, and hydrogen tank are restricted to prevent unrealistic and economically unviable oversizing relative to the peak load demand.

3.3.2. Energy Balance Constraint

The total energy balance of the system for each hour is defined as Equation 23 below.

$$P_{PV}(t) + P_{WT}(t) + P_{FC}(t) + P_{grid,buy}(t) = P_{load}(t) + P_{EL}(t) + P_{grid,sell} \quad (23)$$

Here, P_{PV}, P_{WT}, P_{FC} represent the PV, WT, and FC productions, respectively; P_{EL} represents the energy consumed by the electrolyzer; and $P_{grid,buy}$ and $P_{grid,sell}$ represent the power amounts purchased from and sold to the grid, respectively. This balance ensures that the load (P_{load}) is always met.

3.3.3. Load Coverage Constraint

In hybrid energy systems, energy supply reliability is directly related to the system's ability to meet load demands without interruption. In this study, system reliability is assessed using the Loss of Power Supply Probability (LPSP) indicator. LPSP is defined as the ratio of the periods during which the system cannot meet the load to the total energy demand and is expressed by Equation 24, described-below [28].

$$LPSP = \frac{\sum_{t=1}^{T} max(0, P_{load}(t) - P_{served}(t))}{\sum_{t=1}^{T} P_{load}(t)} \quad (24)$$

Here, $P_{served}(t)$ represents the total generated power (PV+WT+FC+Grid) at time t. T is the total number of time steps ($T = 8760$ in this study, i.e., one year). Minimizing LPSP in the optimization process is important for increasing system reliability.

The LPSP value lies in the range of $0 \leq LPSP \leq 1$. $LPSP = 0$ represents the situation where the system meets the entire load without interruption (fully reliable), $LPSP = 1$ represents the situation where the system cannot meet any load.

In this study, the system is modelled as part of a grid (grid-connected). As explicitly depicted in the revised operational flowchart (Figure 2), when the renewable generation and fuel cell output are insufficient to meet the load, the system control logic automatically triggers the 'Grid Buy' mechanism to supply the deficit power. This ensures that the load demand is fully met at every time step ($P_{served} = P_{load}$), resulting in an annual Loss of Power Supply Probability (LPSP) of zero. A zero $LPSP$ indicates that the system provides full reliability in energy supply.

In off-grid scenarios, achieving $LPSP = 0$ is much more difficult and costly. In this scenario, because there is no grid support, PV, WT, FC, and H_2 storage units must be sized to meet the load year-round. Thus, the system can maintain energy supply solely with its own generation and storage capacity.

As a result, the grid-connected hybrid PV/WT/FC system demonstrated full performance in terms of energy supply reliability under the condition of $LPSP = 0$. This result shows that the COE and HHD values obtained during the optimization process of the system also ensure an uninterrupted energy supply.

4. OPTIMIZATION ALGORITHMS

4.1 Osprey Optimization Algorithm

The Osprey Optimization Algorithm (OOA) is a nature-inspired metaheuristic optimization method introduced in 2023 [47]. This algorithm was developed to solve optimization problems encountered in engineering and other scientific fields. The OOA, models the hunting strategies of ospreys. Among the most significant advantages of the OOA is its ability to effectively manage the exploration and exploitation phases in the search space. This reduces the probability of getting stuck in local minima, resulting in more reliable and consistent solutions [48]. The specific selection and methodological novelty of implementing the OOA for sizing the proposed grid-connected PV/WT/FC system is driven by the highly non-linear, multi-modal, and heavily constrained nature of this problem (e.g., strictly maintaining LPSP = 0 under highly variable meteorological conditions). Traditional metaheuristics, such as PSO and GWO, frequently suffer from premature convergence in such complex multi-objective landscapes because their population diversity diminishes rapidly when dealing with the intermittent profiles of solar and wind resources. Conversely, the OOA offers a compelling advantage and a highly robust solution for this particular application through its mathematically rigorous two-phase mechanism (searching and catching prey). In Phase 1 (exploration), the random selection and position updating mechanism towards the prey (Eq. 29) ensures robust global search capabilities, structurally preventing the algorithm from being trapped in the numerous local optima inherently created by the fluctuating nature of renewable generation. Subsequently, in Phase 2 (exploitation), the algorithm performs a highly focused local search around the safe position (Eq. 31) to fine tune the specific decision variables ($N_{PV}, N_{WT}, P_{FC}, H_2, P_{EL}$). This superior and dynamic balance between broad exploration and precise exploitation overcomes the premature convergence commonly observed in classical methods, making the OOA exceptionally well-suited for resolving the complex trade-offs between minimizing the Cost of Energy (COE) and Human Health Damage (HHD). Ultimately, this unique mechanism yields a denser and more accurate Pareto front than classical algorithms. One of the key components of OOA is the population structure. In OOA, solution candidates are organized using a matrix-based system. In the initial phase of the optimization process, the positions of ospreys within the hunting area are randomly assigned. This random start allows the algorithm to explore a large search space, ensuring diversity is preserved in the early stages. The main steps of the OOA are as follows:

Step 1: Initialization of Ospreys' Positions

At the beginning of the optimization process, the search space and relevant parameters are defined. The initial positions of all ospreys are randomly distributed within the feasible solution space. Each osprey's fitness value, corresponding to the objective function, is calculated according to Equation 25:

$$X = [X_1, X_2, \dots, X_n]^T = \begin{bmatrix} x_{1,1} & \cdots & x_{1,j} & \cdots & x_{1,k} \\ \vdots & \ddots & \vdots & \iddots & \vdots \\ x_{i,1} & \cdots & x_{i,j} & \cdots & x_{i,k} \\ \vdots & \iddots & \vdots & \ddots & \vdots \\ x_{n,1} & \cdots & x_{n,j} & \cdots & x_{n,k} \end{bmatrix} \quad (25)$$

Here, Xi represents the location of the ith osprey, i=1,2,...,n, and n represents the number of ospreys. To ensure that all ospreys are within the specified feasible range, the location of individuals is defined using Equation 26.

$$x_{i,j} = lb_j + r_{i,j}(ub_j - lb_j) \quad (26)$$

Here, ub_j represents the upper bound, lb_j represents the lower bound, and $r_{i,j}$ is a random number in the range [0, 1].

Step 2: Exploration – Searching and Catching Prey

Each osprey is considered a candidate solution to the optimization problem. Therefore, a fitness evaluation must be performed for all ospreys. The value of the fitness function for the corresponding problem is expressed in Equation 27.

$$f(X) = [f(X_1), f(X_2), \cdots, f(X_n)] \quad (27)$$

Here, $f(X_i)$ is the fitness value of the ith osprey.

During the exploration phase, an osprey can precisely locate fish underwater and capture them effectively. It is assumed that the osprey hunts fish underwater until it reaches better objective function values in the search area. In this context, the mathematical model representing the osprey's prey capture process is presented in Equation 28.

$$p_i = \{X_k | k \in \{1,2,\cdots,N\} \wedge f(X_i)\} \cup \{X_{best}\} \quad (28)$$

Here, p_i and X_{best} denote the fish positions and the best candidate position for the i^{th} osprey, respectively. The osprey uses random selection when targeting a fish and uses Equation 29 to calculate its new position as it moves toward the school of fish.

$$x_{i,j}^{p1}(t+1) = x_{i,j}(t) + r_{i,j}\left(s_{i,j} - \zeta \cdot x_{i,j}(t)\right) \quad (29)$$

Here, $x_{i,j}^{p1}$ represents the new position of the osprey in the first stage, t represents the current iterations, and $s_{i,j}$ represents the jth dimension. Furthermore, ζ represents a randomly selected value from the set {1, 2}. If the updated position of the osprey exceeds the specified limits, its new position is redetermined according to Equation 30, taking into account the limit values.

$$x_{i,j}(t+1) = \begin{cases} lb_j, x_{i,j}^{p1}(t+1) < lb_j \\ ub_j, x_{i,j}^{p1}(t+1) > ub_j \end{cases} \quad (30)$$

Step 3: Exploitation – Updating the Best Position

After hunting a fish, ospreys need to find a suitable position. This phase allows the OOA to perform a local search and converge to the optimal solution. The target is positioned at a new location determined as the safe location, according to Equation 31. If the objective function value at this new location improves, the original position is adjusted accordingly. Equation 32 is used for this purpose.

$$x_{i,j}^{p2}(t+1) = x_{i,j}(t) + \frac{lb_j + r_{i,j}(ub_j - l_j)}{t} \quad (31)$$

$$x_{i,j}(t+1) = \begin{cases} lb_j, x_{i,j}^{p2}(t+1) < lb_j \\ ub_j, x_{i,j}^{p2}(t+1) > ub_j \end{cases} \quad (32)$$

The pseudocode syntax of the OOA algorithm is given in Figure 3.

Algorithm **1. The pseudo code of the OOA**

Input: **The population size N, the maximum number of iterations T, the design variables, the objective function, and the upper and lower boundaries.**

Output: **The optimal solutions and the values of the design variables.**

The initialisation of the parameters of the OOA is to be conducted using Eq. (25);
Calculate the values of the fitness function using Eq. (27);
while **stopping criteria ($t \leq T$) is not satisfied** ***do***
  for **each individual in population** ***do***
    Phase 1:
    Calculating the fish positions set for i th osprey using Eq. (28);
    Uptade the position of the i th osprey using Eq. (29);
    if **an osprey exceeds the search space, a new osprey is randomly generated;**
      Update the population using Eq. (30);
    else
      Check the limits of the variables;
    end
    Phase 2:
    Uptade the position of the i th osprey using Eq. (31);
    if **an osprey exceeds the search space, a new osprey is randomly generated;**
      Update the population using Eq. (32);
    else
      Check the limits of the variables;
    end
  end for
  t =t+1;
end while

Figure 3. The OOA's pseudocode.

Table 1 presents the control parameters of the OOA used in the experimental section, as well as those of PSO, TLBO, and GWO for comparison with the proposed algorithm.

Table 1. Control parameters used in different algorithms.

Parameter	PSO	TLBO	GWO	OOA
Population Size	30	30	30	30
Maximum Iterations	200	200	200	200
Number of Decision Variables	5	5	5	5
Inertia Weight (w)	0.7	–	–	–
Cognitive Coefficient (c_1)	1.5	–	–	–
Social Coefficient (c_2)	1.5	–	–	–

5. SIMULATION AND RESULTS

In this study, a renewable energy hybrid system consisting of solar panels, wind turbines, fuel cells, an electrolyzer, hydrogen storage, and a grid was designed and optimized to feed the load. For the optimization study, hourly (over a year) solar radiation, wind speed, temperature, and load data for the Central Anatolia region of Turkey were used, and the changes in these data are shown in Figure 4. In this system, the COE and HHD multi-objective functions were targeted, and the optimization study was calculated according to these objective functions. The system was analyzed

with the OOA algorithm in three different operating scenarios: PV/WT/FC, PV/FC, and WT/FC. The OOA algorithm optimization results are given in Table 2. The PV/WT/FC scenario includes 621 PV panels, 155 wind turbines, and a 40.578 kW fuel cell, supported by a 36.839 kg H_2 tank and a 118.997 kW electrolyzer. The hybrid system created in this scenario balances renewable energy sources, supported by a hydrogen-based fuel cell, resulting in the most balanced system. In other scenarios, where PV and WT are excluded, the number of units increases. While the WT/FC system appears to be the most economical system, the PV/WT/FC scenario stands out as the most ideal system in terms of the COE and HHD objective functions and the balance of renewable energy use. Furthermore, the PV/WT/FC scenario is the only one in which hydrogen technologies are truly used efficiently. This demonstrates why it is the most balanced system in terms of both flexibility and environmental benefits. These different configurations provide the opportunity to analyze the impact of renewable generation sources on the system.

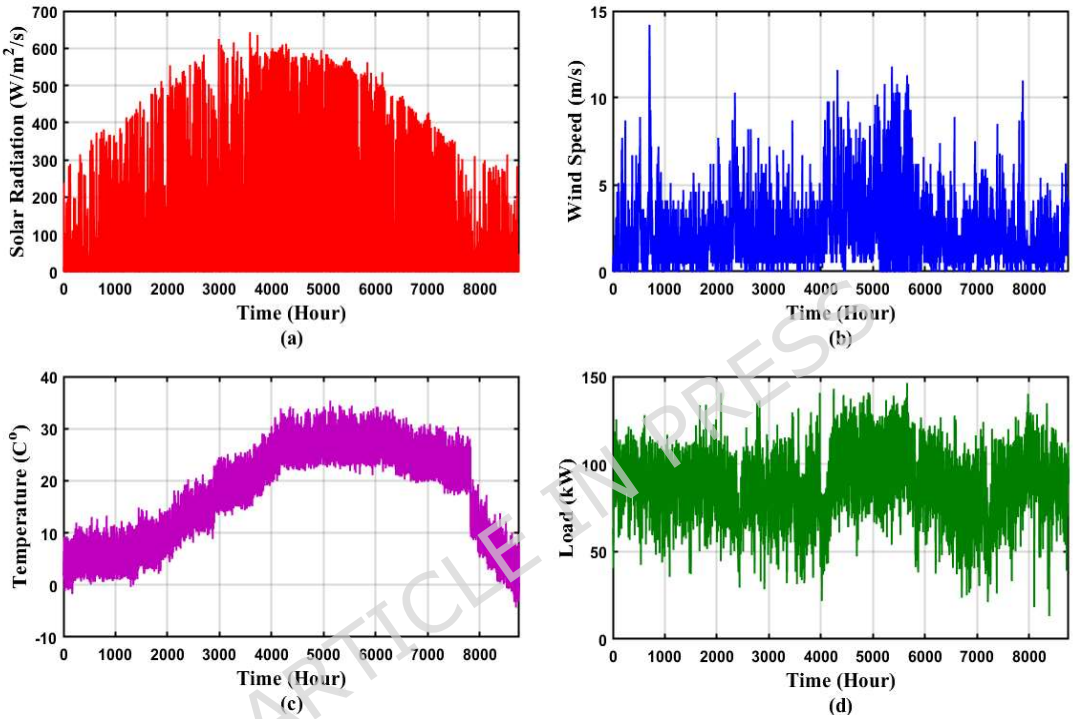

Figure 4. Meteorological data and load graph for the Central Anatolia Region of Türkiye (a) Solar Radiation, (b) Wind Speed, (c) Temperature, (d) Load

Table 2. OOA optimization analysis results.

	OOA		
System Components	PV/WT/FC	PV/FC	WT/FC
PV (Units)	621	932	0
WT (Units)	155	0	179
FC (kW)	40.578	16.161	6.481
H_2 tank (kg)	36.839	20.889	23.790
Electrolyzer (kW)	118.997	85.050	46.162
COE ($/kWh)	0.238	0.248	0.194
HHD (Dalys)	0.419	0.471	0.535

Figure 5 presents a comparison of the COE and HHD values for three different scenarios. When the economic and environmental performance analyses of the scenarios are examined, the COE values for the PV/WT/FC, PV/FC, and WT/FC scenarios are calculated as 0.238, 0.248, and 0.194 $/kWh, respectively. The lowest HHD value was achieved with the PV/WT/FC scenario at 0.419 DALY. In this context, it is observed that PV-based structures offer higher costs than WT-based structures, and that the environmental impact increases when wind turbines are used alone. The fundamental trade-off observed in the WT/FC scenario—achieving the lowest COE (0.194 $/kWh) yet the highest HHD (0.535 DALY)—is physically driven by the system's operational dynamics and grid dependency. While the WT/FC configuration incurs the lowest Net Present Cost (1.872 $ million) due to lower capital requirements for storage and generation units compared to PV-heavy scenarios, the intermittent nature of wind requires substantial grid support to maintain reliability. As detailed in Table 3, the WT/FC scenario necessitates the highest volume of grid energy purchases (628,197 kWh). Since the grid acts as a fossil-fuel-intensive backup, this heavy reliance drastically increases the LCE, thereby elevating the HHD despite the economic savings on initial capital expenditure. Consequently, Table 2 clearly demonstrates the trade-off between cost in one dimension and environmental impact in multi-objective optimization. In this context, optimization using the OOA algorithm shows that the PV/WT/FC scenario is the most suitable hybrid structure when multiple criteria (cost and environmental impact) are considered.

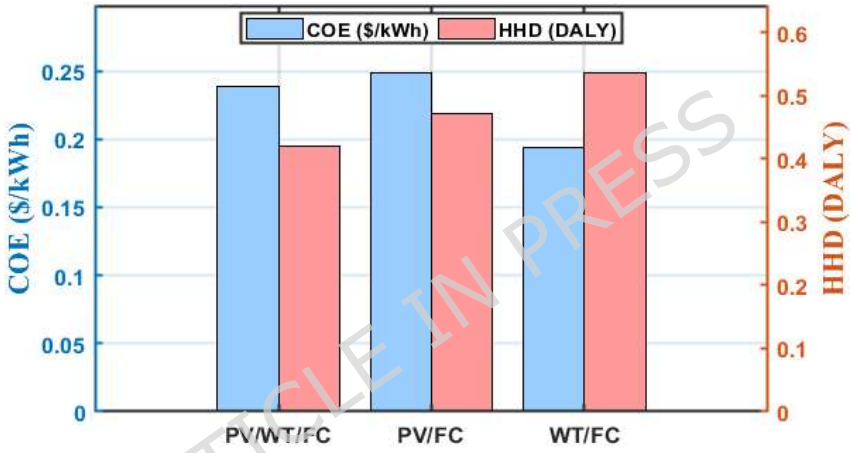

Figure 5. COE and HHD analysis results graph for different scenarios

The Pareto chart results of the multi-objective OOA algorithm study in all scenarios are shown in Figure 6. In the Pareto chart, the most balanced structure is achieved with the PV/WT/FC scenario. When comparing the PV/FC scenario with the PV/WT/FC scenario, the HHD value remains higher and also has a higher cost. Considering the knee point in the Pareto analysis, the most suitable hybrid structure is the PV/WT/FC scenario. This structure is the preferred scenario because it provides the optimal balance between cost and environmental impact.

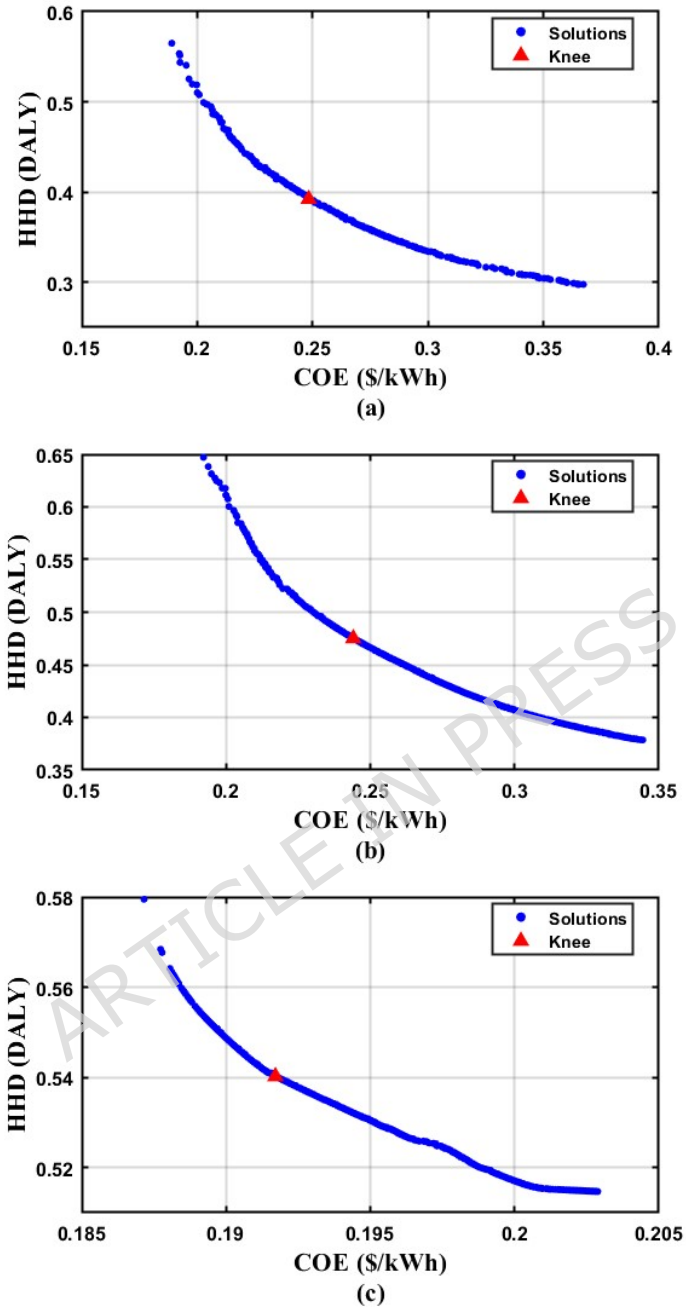

Figure 6. COE–HHD Pareto fronts for hybrid energy systems: (a) PV/WT/FC, (b) PV/FC, and (c) WT/FC.

The Minimum Euclidean Distance method was used to objectively determine the 'knee point' (the optimal trade-off solution) from the non-dominant Pareto set. The knee point is defined by Equation 33 as the solution that minimizes the distance to the 'ideal point' in the normalized objective space.

$$D_i = \sqrt{\left(COE_{n,i}\right)^2 + \left(HHD_{n,i}\right)^2} \quad (33)$$

Where $COE_{n,i}$ and $HHD_{n,i}$ represent the normalized values of the objective functions for the $i.th$ solution.

5.1. Evaluation of Energy Balance Performance

In Figure 7, three subgraphs (a, b, c) show the hourly generation values, grid buy/sell quantities, and load profiles for the PV/WT/FC, PV/FC, and WT/FC scenarios, respectively. June 21st was chosen as the longest daylight value. In Figure 7(a), in the PV/WT/FC scenario, the generation profile varies throughout the day, with both PV and WT contributions. Grid sell occurs in the morning and afternoon hours (6–14), indicating that generation exceeds load demand. Consequently, this scenario offers a balanced structure that can meet the majority of the load with renewable resources and sell the daytime surplus to the grid. In Figure 7(b), in the PV/FC scenario, generation is largely dependent on solar energy (PV). While high generation is achieved in the afternoon hours (9–15), generation is almost absent in the morning and evening hours. Therefore, grid buy is concentrated in the morning hours, when the load is low. Ultimately, this system exhibits a strong solar presence but a weak sustainability profile, exhibiting a high grid dependency profile. In Figure 7(c), in the WT/FC scenario, generation relies entirely on wind energy (WT). Wind generation is consistently high throughout the day. Because generation far exceeds demand, there is a constant supply of electricity to the grid (Grid Sell). While this system offers cost advantages, its health impact is higher because it relies on a constant overproduction and overselling mechanism.

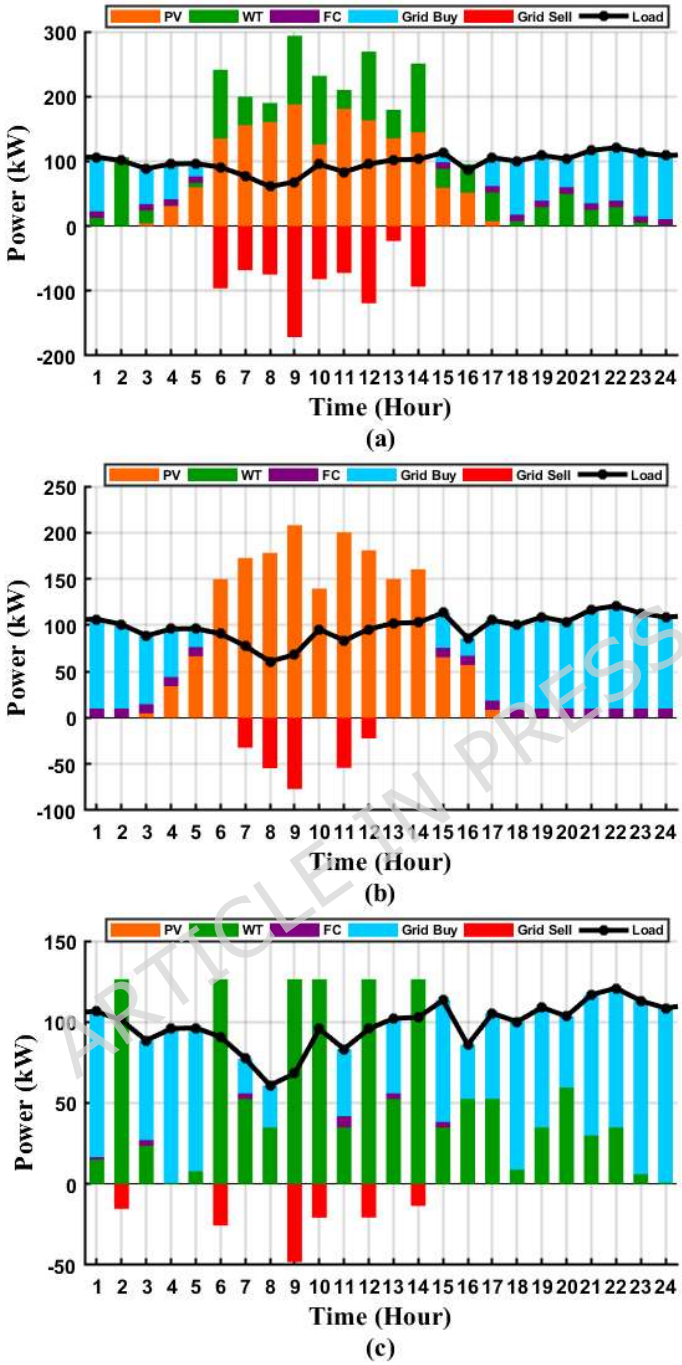

Figure 7. Hourly production values, grid buying/selling quantities, and load profile according to the OOA algorithm analysis results (a) PV/WT/FC, (b) PV/FC, (c) WT/FC

5.2. Total Production and Productivity Evaluation

Table 3 presents the total energy production and efficiency assessment ratios for one year (8,760 hours) for three different hybrid energy scenarios (PV/WT/FC, PV/FC, and WT/FC). The data reveals significant differences in the systems' renewable contributions, grid dependency, and overall efficiency levels. Comparing the production profiles of all scenarios, the PV/WT/FC scenario produces 177148.296 kWh from PV, 236053.817 kWh from WT, and 34997.467 kWh

from FC. In other words, production diversity is high, and the PV–WT contribution is balanced. In the PV/FC scenario, PV production is high (266100.556 kWh), but there is no WT, and FC contribution is limited (23857.148 kWh). Therefore, it is a solar-dependent structure. In the WT/FC scenario, production is largely based on WT (272292.078 kWh), FC production is relatively low (12842.421 kWh), and PV is entirely absent. Consequently, the PV/WT/FC system provides more balanced and diversified production, while the other scenarios appear to be dependent on a single source. When comparing the energy sold and received to the grid, the PV/WT/FC scenario receives 482167.549 kWh from the grid, while 61047.246 kWh are sold to the grid. Net grid dependency is 54.38%, making it the least grid-dependent system. The highest electrical efficiency (ηsys) was achieved with the WT/FC scenario at 96.55%. The highest load response efficiency (ηload) was achieved with the PV/FC scenario at 92.49%. In terms of efficiency, PV/FC provides the best load matching; WT/FC is technically highly efficient but limited in load response. The PV/WT/FC system has the highest values among the scenarios in terms of renewable penetration, self-sufficiency ratio (SSR), and H_2 share, at 57.88%, 37.74%, and 10.20%, respectively. In this context, the PV/WT/FC system is the strongest in terms of renewable contribution and self-sufficiency. A general assessment based on Table 3 shows that PV/WT/FC is the best scenario for energy diversity and sustainability, while PV/FC and WT/FC are the best scenarios in terms of efficiency and load response. While PV/FC and WT/FC may be advantageous in terms of cost/efficiency, they are the weakest scenarios in terms of sustainability and independence.

Table 3. Total production and productivity values in all scenarios according to the analysis results of the algorithms.

	PV/WT/FC	**PV/FC**	**WT/FC**
PV (kWh)	177148.926	266100.556	0
WT (kWh)	236053.817	0	272292.078
FC (kWh)	34997.467	23857.148	12842.421
Grid_in (kWh)	482167.549	547329.179	628197.370
Grid_out (kWh)	61047.246	648.095	107464.809
Electrolyzer (kWh)	94943.114	62261.388	31489.660
Load (kWh)	774377.400	774377.400	774377.400
System electrical efficiency (ηsys) (%)	89.795	92.564	96.552
Load coverage efficiency (ηload) (%)	83.233	92.487	84.786
Renewable penetration (%)	57.879	37.444	36.821
Net grid dependency (%)	54.382	70.596	67.245
Self-sufficiency ratio (SSR) (%)	37.735	29.320	18.877
H_2 share (Fraction of renewable power directed to electrolysis) (%)	10.205	7.436	3.448

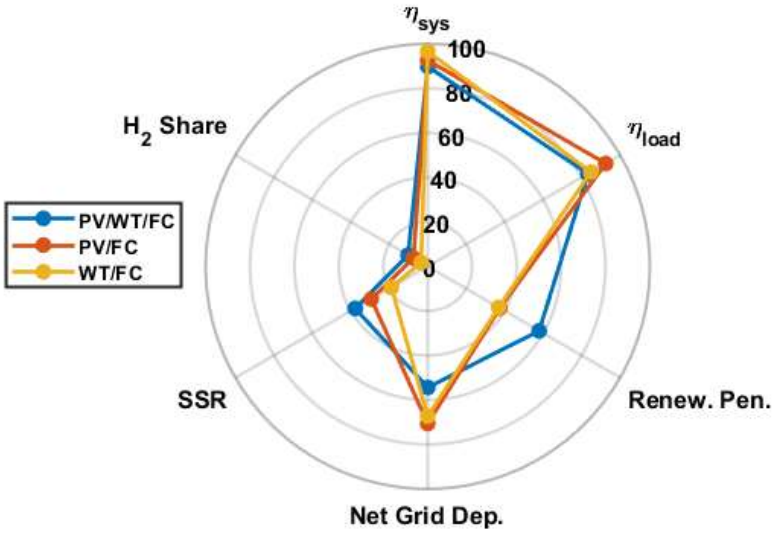

Figure 8. Performance indicator radar chart of three different hybrid systems (PV/WT/FC, PV/FC, WT/FC).

Figure 8 compares the PV/WT/FC, PV/FC, and WT/FC scenarios using a radar chart of hybrid energy system performance indicators. The PV/WT/FC system stands out in renewable energy penetration, self-sufficiency ratio, and H_2 share, while the PV/FC scenario performs best in load response and system efficiency. While the WT/FC system has the highest electrical efficiency, it is the weakest scenario in terms of renewable energy contribution and self-sufficiency.

5.3. Cost Analysis

Figure 9 presents a comparative cost analysis of hybrid energy systems for three scenarios. In the PV/WT/FC scenario, the Net Present Cost (NPC) of the total investment is calculated as \$2.299 million, and the unit energy cost (COE) is \$0.238/kWh. The PV/FC scenario is the most cost-effective option, with an NPC of \$2.395 million and a COE of \$0.248/kWh, higher than the other scenarios. In contrast, the WT/FC scenario is the most economical solution, with an NPC of \$1,872 million and a COE of \$0.194/kWh.

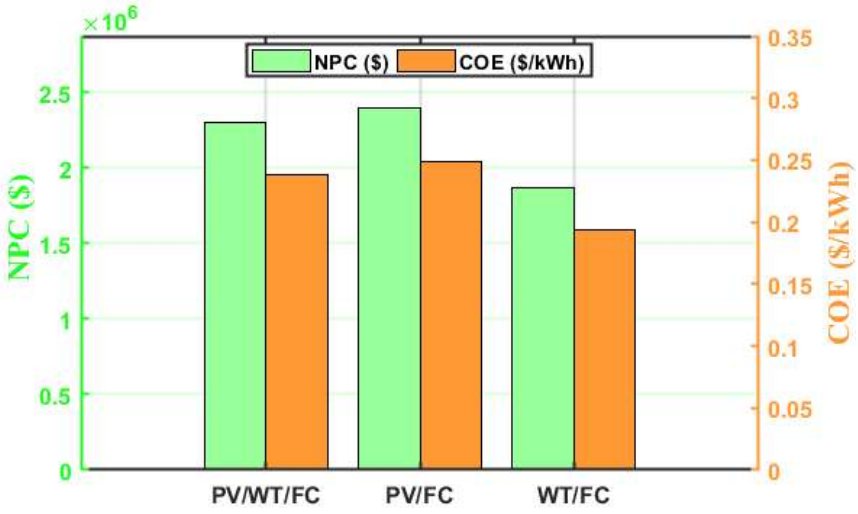

Figure 9. NPC and COE graphs in different scenarios.

In Figure 10, when the cost distribution by component is examined, the majority of the cost in the PV/FC scenario stems from PV (\$0.908 M) and FC (\$0.049 M) investments. In the WT/FC scenario, the WT component is the dominant

cost element ($0.311 M), and the INV component is the dominant cost element ($0.128 M). The PV/WT/FC scenario, on the other hand, has a more balanced cost distribution, presenting a diversified structure with investments in PV ($0.605 M), WT ($0.270 M), FC ($0.123 M), H_2 tank ($0.021 M), and inv ($0.186 M). These results reveal that PV/FC is the most expensive, WT/FC the most economical, and PV/WT/FC is a mid-range option that is more balanced and sustainable.

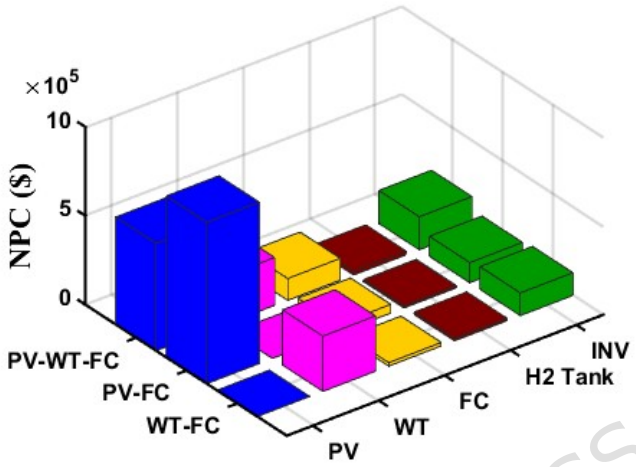

Figure 10. Cost distribution by components in different scenarios.

5.4. Environmental Analysis

Figure 11 shows the total HHD (DALY) and LCE (kg CO_2-eq/yr) values of the PV/WT/FC, PV/FC, and WT/FC hybrid systems, and quantitatively analyzes their environmental and health impacts. The lowest HHD value of 0.419 DALY was obtained for the PV/WT/FC system, indicating that its adverse effects on human health are minimal compared to other configurations. The HHD value increased to 0.471 DALY for the PV/FC system and to 0.535 DALY for the WT/FC system. Similarly, the LCE value representing life-cycle carbon emissions was determined to be approximately 2.995×10^5 kg CO_2-eq/yr for the PV/WT/FC system, 3.364×10^5 kg CO_2-eq/yr for the PV/FC system, and 3.824×10^5 kg CO_2-eq/yr for the WT/FC system. These findings clearly demonstrate that the PV/WT/FC configuration, where PV and WT sources are used together, offers the most environmentally friendly solution in terms of both lower emissions and health impacts.

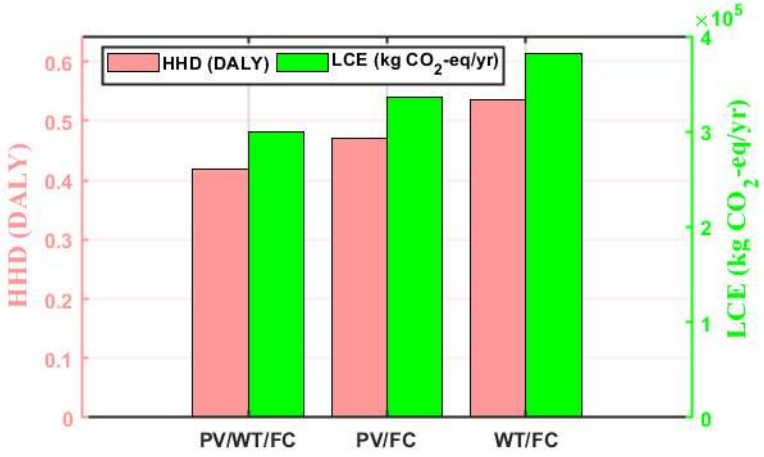

Figure 11. Total HHD and LCE graph in different scenarios.

Figure 12 presents a comparison of the annual carbon emission equivalent (LCE, kg CO_2-eq/yr) values of the system components and the grid by scenario type. According to the results, the grid stands out as the component with the highest emission value in all scenarios. It accounts for the majority of the total LCE with values of 2.893×10^5, 3.284×10^5, and 3.769×10^5 kg CO_2-eq/yr in the PV/WT/FC, PV/FC, and WT/FC scenarios, respectively. Among the renewable components, PV modules had values of 5.314 kg CO_2-eq/yr in the PV/WT/FC scenario and 7.983 kg CO_2-eq/yr in the PV/FC scenario, while the WT/FC scenario produced zero values due to the absence of PV. WT, on the other hand, exhibited emission levels similar to the PV component, with values of 4721 kg CO_2-eq/yr in the PV/WT/FC scenario and 5446 kg CO_2-eq/yr in the WT/FC scenario. The FC component has a very low environmental impact in all scenarios, with values of 174.99, 119.29, and 64.21 kg CO_2-eq/yr, respectively, which are negligible compared to the other components. Overall, the PV/WT/FC scenario stands out as the most environmentally friendly solution in terms of total LCE, and in this scenario, where grid dependency decreases, the share of renewable resources in energy production increases significantly. Conversely, the increase in grid utilization in the PV/FC and especially the WT/FC scenarios led to a significant rise in carbon emissions. This finding demonstrates that reducing grid interaction in hybrid systems is critical for environmental sustainability.

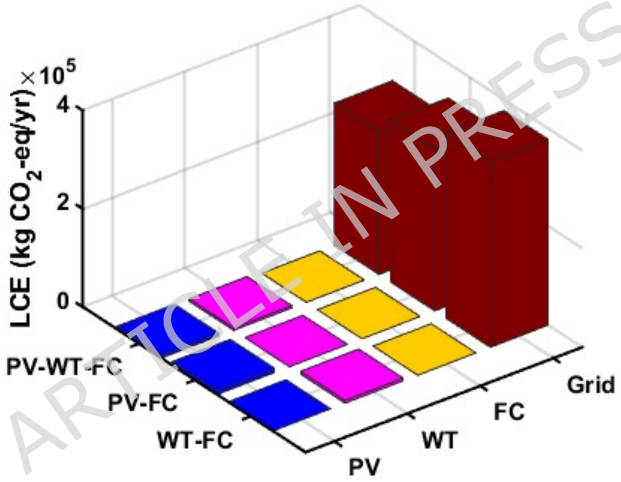

Figure 12. Carbon emission distribution by components in different scenarios.

5.5. Comparative analysis of the developed algorithm

To demonstrate the effectiveness of OOA, the hybrid power system was also tested with the PSO, TLBO, and GWO algorithms. Table 4 shows the results of the hybrid energy system obtained with different optimization algorithms (PSO, TLBO, GWO, and OOA). The highest PV capacity was found to be 1.136 units in the GWO algorithm, while the lowest value was 621 units in OOA. WT capacity reached a maximum of 200 units in GWO, and a more balanced value was achieved in OOA at 155. In terms of FC capacity, the OOA algorithm provided the highest value at 40.58 kW, while PSO produced only 6.74 kW. While the H_2 tank capacity reached its highest level in TLBO at 115.78 kg, OOA determined a more optimal storage requirement of 36.84 kg. The electrolyzer capacity reached its highest level in OOA at 118.99 kW, increasing the system's flexibility. When performance indicators are evaluated, the lowest COE, i.e., the most economical solution, was achieved with OOA, with a COE of $0.238/kWh. Although OOA produces a relatively high value of 0.419 DALY in terms of HHD, the overall efficiency of the system is increased thanks to its cost advantage. Overall, the results reveal that the OOA algorithm offers the best optimization performance with the lowest energy cost and balanced component sizing compared to other methods. Highlighting the novelty of this work, the comparative

analysis clearly demonstrates that the newly applied OOA successfully escapes the local minima that typically restrict traditional algorithms. This results in a much denser and more accurate Pareto front (Figure 13d), providing decision-makers with a truly optimal and novel sizing balance between COE and HHD.

Table 4. Optimization analysis results of algorithms.

Component	**PSO**	**TLBO**	**GWO**	**OOA**
PV (Piece)	884	927	1136	621
WT (Piece)	121	112	200	155
FC (kW)	6.741	33.477	37.798	40.578
H_2 tank (kg)	33.854	115.784	72.555	36.839
Electrolyzer (kW)	64.110	64.777	120	118.997
COE ($/kWh)	0.246	0.259	0.280	0.238
HHD (DALY)	0.413	0.402	0.352	0.419

Figure 13 shows the Pareto fronts for multi-objective optimization of hybrid energy systems. Blue dots indicate Pareto-optimal solutions, and red triangles indicate knee points. Figure 13(a) shows the Pareto solution graphs for the PSO algorithm, Figure 13(b) for the TLBO algorithm, Figure 13(c) for the GWO algorithm, and Figure 13(d) for the OOA algorithm. In graphs (a) and (c), the solution space is large, but HHD reaches higher levels. In graph (b), the solution set is sparsely distributed, limiting the accuracy of the knee point. In contrast, graph (d) presents the most regular and dense Pareto front, with the knee point determined at a cost of approximately $0.24/kWh and a health impact of 0.38 DALY. This result demonstrates that in graph (d), the OOA algorithm represents the most optimal solution in terms of cost-health balance and the most advantageous solution for decision makers.

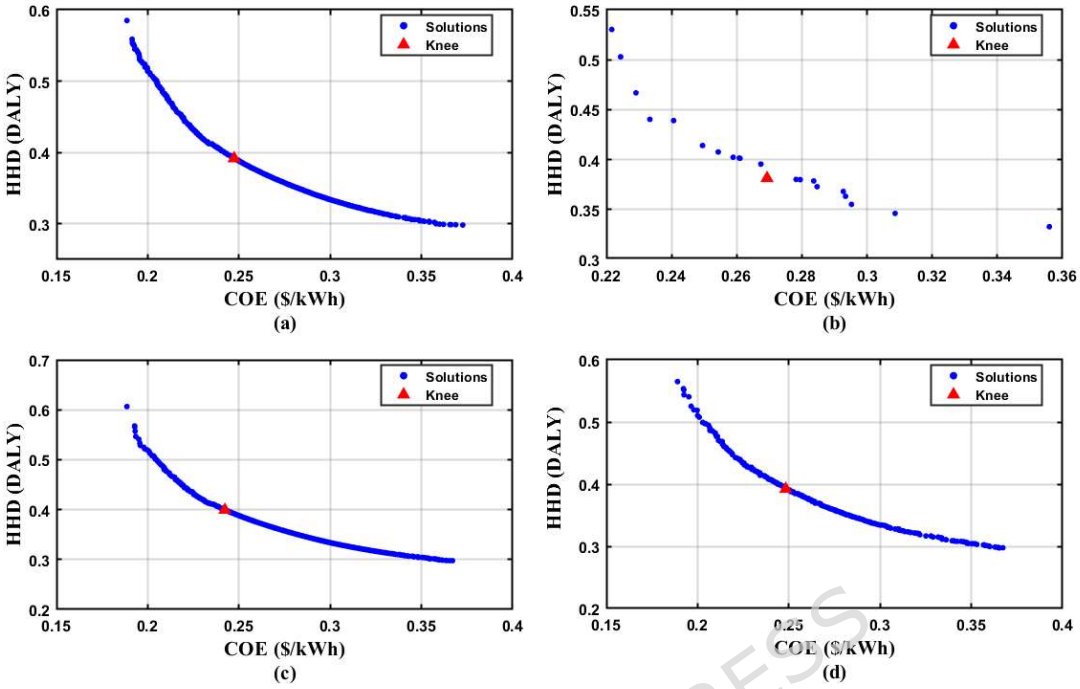

Figure 13. Pareto fronts of multi-objective optimization of hybrid energy systems, (a) PSO, (b) TLBO, (c) GWO, and (d) OOA.

To validate the reliability of the obtained results, the optimal COE (0.238 $/kWh) achieved by the OOA for the PV/WT/FC system was compared with similar hybrid system studies in the literature. For instance, Samy et al. [21] reported COE values of 0.45 $/kWh using the Firefly Algorithm and 0.51 $/kWh using the PSO algorithm for a similar configuration in Egypt. The variation in COE values obtained in this study is attributed to three main factors: firstly, the grid-connected architecture allows for the sale of excess energy, effectively offsetting operational costs; secondly, the superior convergence capability of the OOA, which successfully identified a more cost-effective sizing combination; and thirdly, the site-specific meteorological conditions. The differences in solar irradiance, wind speed profiles, and load demand specific to the Central Anatolia region naturally yield different component sizing and economic outcomes compared to the climatic datasets used in the referenced studies.

6. CONCLUSION

This study presented a comprehensive multi-objective optimization framework for a grid-connected hybrid renewable energy system (HRES) powered by PV, wind, and hydrogen technologies. By applying the Osprey Optimization Algorithm (OOA), the study successfully minimized both the Cost of Energy (COE) and Human Health Damage (HHD) while ensuring zero loss of power supply probability (LPSP = 0). Quantitatively, the simulation results identified the PV/WT/FC configuration as the most balanced Pareto-optimal solution among the investigated scenarios. This configuration achieved a highly competitive COE of 0.238 $/kWh and the lowest environmental impact with an HHD of 0.419 DALY. In contrast, while the wind-dominated (WT/FC) scenario offered the lowest cost (0.194 $/kWh), it resulted in the highest health damage (0.535 DALY) due to a heavy grid dependency of 67.2%. The optimized PV/WT/FC system significantly improved sustainability, achieving a renewable penetration rate of 57.88 % and reducing net grid dependency to 54.38 %, thereby validating the effectiveness of integrating hydrogen storage. Qualitatively, the comparative analysis demonstrated that OOA provides superior convergence stability and solution quality compared to PSO, TLBO, and GWO algorithms. The OOA-based approach effectively avoided premature convergence in the

complex, multi-modal search space of the hybrid system, resulting in a denser and more accurate Pareto front. Ultimately, the primary novelty of this research lies in successfully applying the OOA to a complex, multi-objective hydrogen-based HRES sizing problem for the first time, whilst distinctly incorporating Human Health Damage (HHD) into the environmental assessment. By addressing the specific gap in utilizing advanced meta-heuristics for health-focused sustainability metrics, this study establishes a novel, highly efficient framework that outperforms traditional algorithms. Future work will focus on integrating stochastic uncertainty modeling for renewable generation and developing AI-based predictive control strategies to further enhance real-time system management.

Declaration of generative AI and AI-assisted technologies in the writing process

During the preparation of this work, the author(s) used an artificial intelligence tool to improve the language and readability of the study. After using this tool/service, the author(s) reviewed and edited the content as needed and took(s) full responsibility for the content of the publication.

Funding: NA

Data availability statement: The dataset is extracted from the NASA Power database that is available at: https://power.larc.nasa.gov/data-access-viewer/

Acknowledgements: NA

Conflicts of interest: The authors declare that they have no conflicts of interest.

Author's Contribution: All authors, Salih ERMİŞ (**SE**), Oğuz TAŞDEMİR (**OT**), and Rami AL-HAJJ (**RH**), contributed significantly to the development of this manuscript and approved the final version for submission. The particular contributions are as follows: All authors contributed to formulating the research idea, objectives, and the study's scope. SE and OT maintain data collection, organization, and validation. Formal analysis is conducted and validated by all authors. SE and OT initiated the investigation and Methodology. Project administration is mainly assured by **SE**. The authors collaborated in coding, running simulations, and validating the optimization models and performance assessments. Resources are mainly maintained by **OT**. Supervision of the work and preparation is conducted by **SE** and **OT**, and the validation is assured by RH. The initial manuscript draft, including the introduction, methodology, results, and discussion sections, was prepared collaboratively by **SE** and **OT**. All authors contributed to revising and refining the manuscript to improve clarity, technical accuracy, and scientific rigor.

References

1. Yi J, Dai S, Li L, Cheng J (2024) How does digital economy development affect renewable energy innovation? *Renewable and Sustainable Energy Reviews*. 192:114221.

2. Sánchez A, Zhang Q, Martín M, Vega P (2025) Towards a new renewable power system using energy storage: An economic and social analysis. *Energy Conversion and Management* 252:115056.

3. Karimi H (2024) A tri-objectives scheduling model for renewable-hydrogen-based microgrid system considering hydrogen storage system and demand-side management. *International Journal of Hydrogen Energy* 68:1412–22.

4. Esen H, Inalli M, Esen M (2006) Technoeconomic appraisal of a ground source heat pump system for a heating season in eastern Turkey. *Energy Conversion and Management* 47:1281–97.

5. Bouendeu JJ, Konchou FAT, Astrid MNB (2023) Elmorshedy MF, René T. A systematic techno-enviro-socio-

economic design optimization and power quality of hybrid renewable microgrids. *Renewable Energy* 218:119297.

6. Dincer I (2007) Environmental and sustainability aspects of hydrogen and fuel cell systems. *International Journal of Energy Research* 31:29–55.

7. Bezmalinović D, Barbir F, Tolj I (2013) Techno-economic analysis of PEM fuel cells role in photovoltaic-based systems for the remote base stations. *International journal of hydrogen energy* 38:417–25.

8. Cin R, Onaygil S, Gökçek T (2024) An ex-ante cost-benefit assessment of the possible Energy Efficiency Obligation Scheme in Türkiye. *Energy Policy* 195:114398.

9. Manoo MU, Shaikh F, Kumar L, Arıcı M (2024) Comparative techno-economic analysis of various stand-alone and grid connected (solar/wind/fuel cell) renewable energy systems. *International Journal of Hydrogen Energy* 52:397–414.

10. Thanaa F, Eskander MN, El-Hagry MT (2006) Energy flow and management of a hybrid wind/PV/fuel cell generation system. *Energy conversion and management* 47:1264–80.

11. Yahya W, Saied KM, Nassar A, Qader M, Al-Nehari M, Zarabia J, et al. (2024) Optimization of a hybrid renewable energy system consisting of a of PV/wind turbine/battery/fuel cell integration and component design. *International Journal of Hydrogen Energy* 94:1406–18.

12. Güven AF, Yörükeren N (2024) A comparative study on hybrid GA-PSO performance for stand-alone hybrid energy systems optimization. *Sigma Journal of Engineering and Natural Sciences* 42:1410–38.

13. Singh S, Chauhan P, Singh N (2020) Capacity optimization of grid connected solar/fuel cell energy system using hybrid ABC-PSO algorithm. *International Journal of Hydrogen Energy* 45:10070–88.

14. Maleki A, Pourfayaz F, Ahmadi MH (2016) Design of a cost-effective wind/photovoltaic/hydrogen energy system for supplying a desalination unit by a heuristic approach. *Solar Energy* 139:666–75.

15. Diab AAZ, Sultan HM, Mohamed IS, Kuznetsov ON, Do TD (2019) Application of different optimization algorithms for optimal sizing of PV/wind/diesel/battery storage stand-alone hybrid microgrid. *IEEE Access* 7:119223–45.

16. Singh P, Pandit M, Srivastava L (2023) Multi-objective optimal sizing of hybrid micro-grid system using an integrated intelligent technique. *Energy* 269:126756.

17. Sawle Y, Gupta S, Bohre AK (2017) Optimal sizing of standalone PV/Wind/Biomass hybrid energy system using GA and PSO optimization technique. *Energy Procedia* 117:690–8.

18. Wandhare RG, Thale S, Agarwal V (2013) Reconfigurable hierarchical control of a microgrid developed with PV, wind, micro-hydro, fuel cell and ultra-capacitor. *Twenty-Eighth Annual IEEE Applied Power Electronics Conference and Exposition (APEC)* 2799–806..

19. Abedi S, Ahangar HG, Nick M, Hosseinian SH (2011) Economic and reliable design of a hybrid PV-wind-fuel

cell energy system using differential evolutionary algorithm. *19th Iranian Conference on Electrical Engineering* 1–6.

20. Das M, Singh MAK, Biswas A (2019) Techno-economic optimization of an off-grid hybrid renewable energy system using metaheuristic optimization approaches–case of a radio transmitter station in India. *Energy conversion and management* 185:339–52.

21. Samy M, Barakat S, Ramadan H (2020) Techno-economic analysis for rustic electrification in Egypt using multi-source renewable energy based on PV/wind/FC. *International Journal of Hydrogen Energy* 45:11471–83.

22. Tito S, Lie T, Anderson T (2016) Optimal sizing of a wind-photovoltaic-battery hybrid renewable energy system considering socio-demographic factors. *Solar Energy* 136:525–32.

23. Dhaliwal NK, Bouffard F, O'Malley MJ (2020) A fast flexibility-driven generation portfolio planning method for sustainable power systems. *IEEE Transactions on Sustainable Energy* 12:368–77.

24. Fodhil F, Hamidat A, Nadjemi O (2019) Potential, optimization and sensitivity analysis of photovoltaic-diesel-battery hybrid energy system for rural electrification in Algeria. *Energy* 169:613–24.

25. Kharrich M, Mohammed OH, Alshammari N, Akherraz M (2021) Multi-objective optimization and the effect of the economic factors on the design of the microgrid hybrid system. *Sustainable Cities and Society* 65:102646.

26. Sanajaoba S (2019) Optimal sizing of off-grid hybrid energy system based on minimum cost of energy and reliability criteria using firefly algorithm. *Solar Energy* 188:655–66.

27. Kaviani AK, Riahy G, Kouhsari SM (2009) Optimal design of a reliable hydrogen-based stand-alone wind/PV generating system, considering component outages. *Renewable energy* 34:2380–90.

28. Koholé YW, Fohagui FCV, Ngouleu CAW, Tchuen G (2024) An effective sizing and sensitivity analysis of a hybrid renewable energy system for household, multi-media and rural healthcare centres power supply: a case study of Kaele, Cameroon. *International Journal of Hydrogen Energy* 49:1321–59

29. Ngouleu CAW, Koholé YW, Fohagui FCV, Tchuen G (2023) Techno-economic analysis and optimal sizing of a battery-based and hydrogen-based standalone photovoltaic/wind hybrid system for rural electrification in Cameroon based on meta-heuristic techniques. *Energy Conversion and Management* 280:116794.

30. Sultan HM, Diab AAZ, Oleg NK, Irina SZ (2018) Design and evaluation of PV-wind hybrid system with hydroelectric pumped storage on the National Power System of Egypt. *Global Energy Interconnection* 1:301–11.

31. Ayodele T, Mosetlhe T, Yusuff A, Ogunjuyigbe A (2021) Off-grid hybrid renewable energy system with hydrogen storage for South African rural community health clinic. *International Journal of Hydrogen Energy* 46:19871–85.

32. Tooryan F, HassanzadehFard H, Collins ER, Jin S, Ramezani B (2020) Optimization and energy management of distributed energy resources for a hybrid residential microgrid. *Journal of Energy Storage* 30:101556.

33. HassanzadehFard H, Jalilian A (2018) Optimal sizing and location of renewable energy based DG units in

distribution systems considering load growth. *International Journal of Electrical Power & Energy Systems* 101:356–70.

34. Vendoti S, Muralidhar M, Kiranmayi R (2018) Design and analysis of solar PV-fuel cell-battery based hybrid renewable energy system (HRES) for off-grid electrification in rural areas. *i-Manager's Journal on Instrumentation & Control Engineering* 6:1.

35. El-Shater TF, Eskander MN, El-Hagry MT (2006) Energy flow and management of a hybrid wind/PV/fuel cell generation system. *International Journal of Sustainable Energy* 25:91–106.

36. Strunz K, Brock EK (2006) Stochastic energy source access management: Infrastructure-integrative modular plant for sustainable hydrogen-electric co-generation. *International journal of hydrogen energy* 31:1129–41.

37. Felseghi R-A, Carcadea E, Raboaca MS, Trufin CN, Filote C (2019) Hydrogen fuel cell technology for the sustainable future of stationary applications. *Energies* 12:4593.

38. Garcia RS, Weisser D (2006) A wind–diesel system with hydrogen storage: Joint optimisation of design and dispatch. *Renewable energy* 31:2296–320.

39. Diab AZ, El-ajmi SI, Sultan HM, Hassan YB (2019) Modified farmland fertility optimization algorithm for optimal design of a grid-connected hybrid renewable energy system with fuel cell storage: Case study of Ataka. *Egypt. Int J Adv Comput Sci Appl*. 10:119–32.

40. Khan MJ, Iqbal MT (2005) Pre-feasibility study of stand-alone hybrid energy systems for applications in Newfoundland. *Renewable energy* 30:835–54.

41. Hassan R, Das BK, Hasan M (2022) Integrated off-grid hybrid renewable energy system optimization based on economic, environmental, and social indicators for sustainable development. *Energy* 250:123823.

42. Baneshi M, Hadianfard F (2016) Techno-economic feasibility of hybrid diesel/PV/wind/battery electricity generation systems for non-residential large electricity consumers under southern Iran climate conditions. *Energy Conversion and Management* 127:233–44.

43. Luna-Rubio R, Trejo-Perea M, Vargas-Vázquez D, Ríos-Moreno G (2012) Optimal sizing of renewable hybrids energy systems: A review of methodologies. *Solar energy* 86:1077–88.

44. Das BK, Al-Abdeli YM, Kothapalli G (2017) Optimisation of stand-alone hybrid energy systems supplemented by combustion-based prime movers. *Applied energy* 196:18–33.

45. Shi Y, Yuan X, Tang Y, Li Y, Wang Q, Ma Q, et al. (2022) Localized regional life cycle model research for the impacts of carbon dioxide on human health and ecosystem. *Sustainable Production and Consumption* 29:36–45.

46. Hussam, W.K., et al. (2025) Techno-economic and environmental evaluation of integrated microgrid systems for electrification and hydrogen production. *in Journal of Physics: Conference Series* IOP Publishing.

47. Dehghani M, Trojovský P (2023) Osprey optimization algorithm: A new bio-inspired metaheuristic algorithm for solving engineering optimization problems. *Frontiers in Mechanical Engineering* 8:1126450.

48. Ismaeel AA, Houssein EH, Khafaga DS, Abdullah Aldakheel E, AbdElrazek AS, Said M (2023) Performance of osprey optimization algorithm for solving economic load dispatch problem. *Mathematics* 11:4107.

49. Jaman A, Al Mahmud R, Das BK, Tushar MSH (2025) Optimizing an integrated hybrid energy system with hydrogen-based storage to develop an off-grid green community for sustainable development in Bangladesh. *International Journal of Hydrogen Energy* 97:766–86.

50. Abu SM, Hannan M, Rahman S, Long CY, Ker PJ, Wong RT, et al. (2025) An effective optimization algorithm for hydrogen fuel cell-based hybrid energy system: A sustainable microgrid approach. *International Journal of Hydrogen Energy* 98:1341–55.

51. Hussam WK, Abdul-Niby M, Sheard GJ (2024) Techno-economic analysis and optimization of hydrogen production from renewable hybrid energy systems: Shagaya renewable power plant-Kuwait. *International Journal of Hydrogen Energy* 58:56–68.

52. Choudhary P, Akella AK (2024) Techno-economic-eco design and investigation of hybrid energy generation systems in tropics. *Iranian Journal of Science and Technology, Transactions of Electrical Engineering* 48:1007–22.

53. Senthilkumar T, Jayasankar T (2026) Optimal sizing of Hybrid Solar-Wind Battery System (HSWBS) using secretary bird optimization. *Electric Power Systems Research* 251:112284.

Supplementary Material

Table A. Techno-economic-environmental data values of HRES system components [49-53].

Compo-nent	Description	Unit	Value
PV	PV panel efficiency	-	0.204
	System performance ratio	-	0.88
	Temperature coefficient (power change)	1/°C	-0.0035
	Nominal operating cell temperature	°C	45
	Power of one PV module	kW	0.327
	Connection cost coefficient	-	0.002
	Investment cost ($/kW)	$/kW	850
	Operation & maintenance cost ($/kW·yr)	$/kW·yr	10
	Lifetime	Years	25
	Emission factor (ε)	kg CO_2-eq/kWh	0.03
WT	Rated power of one wind turbine	kW	2
	Connection cost coefficient	-	0.5

	Investment cost ($/kW)	$/kW	1300
	Operation & maintenance cost ($/kW·yr)	$/kW·yr	35
	Lifetime	Years	20
	Emission factor (ε)	kg CO_2-eq/kWh	0.02
FC	Fuel cell efficiency	-	0.5
	Investment cost ($/kW)	$/kW	2200
	O&M ratio (fraction of CapEx)	-	0.03
	Lifetime	Years	7
	Salvage value	$	500
	Emission factor (ε)	kg CO_2-eq/kWh	0.005
H_2 Tank	Higher heating value of hydrogen	kWh/kg	39.4
	Investment cost ($/kg)	$/kg	450
	O&M ratio (fraction of CapEx)	-	0.02
	Lifetime	Years	20
Electro-lyzer	Electrolyzer efficiency	-	0.75
	Investment cost ($/kW)	$/kW	900
	Operation & maintenance cost ($/kW·yr)	$/kW·yr	20
	Lifetime	Years	15
Inverter	Inverter efficiency	-	0.96
	Investment cost ($/kW)	$/kW	300
	O&M ratio (fraction of CapEx)	-	0.015
	Lifetime	Years	15
	Salvage value	$	50
General	Grid electricity purchase price	$/kWh	0.12
	Grid electricity selling price	$/kWh	0.05
	Discount rate	-	0.05
	Project lifetime	Years	20